Advanced Steel Construction – Vol. 18 No. 3 (2022) 707–714
DOI:10.18057/IJASC.2022.18.3.8

MECHANICAL BEHAVIOUR OF CORRODED STRUCTURAL STEEL SUBJECTED TO MONOTONIC TENSION

Qi Si [1], Yang Ding [1, 2], Liang Zong [1, 2, *] and Hua-Tian Zhao [3]

[1] *School of Civil Engineering, Tianjin Univ., Tianjin 300072, China.*
[2] *Key Laboratory of Coast Civil Structure Safety, Ministry of Education, Tianjin Univ., Tianjin 300072, China*
[3] *Key Laboratory of Civil Engineering Safety and Durability of China Education Ministry, Tsinghua University, Beijing 100084, China*
** (Corresponding author: E-mail: zongliang@tju.edu.cn)*

ABSTRACT

This study aims to investigate the mechanical properties of corroded structural steel under monotonic tensile loading. First, structural steel coupons with various corrosion degrees were produced by electrolytic accelerated corrosion using a particular etchant solution proposed by the authors. Second, the corroded morphologies of the specimens were observed through a morphology scanner; then, the mechanical properties were examined by monotonic tensile loading tests. An analytical model on the relationship between mass loss and surface morphology with the mechanical properties of corroded structural steel was established. Finally, a numerical simulation method was proposed on the mechanical behaviour of corroded structural steel based on random rough surface theory. The finite element was consistent with experimental tests, which indicates the feasibility and accuracy of the proposed simulation method.

ARTICLEHISTORY

Received: 11 August 2021
Revised: 22 January 2022
Accepted: 31 January 2022

KEYWORDS

Accelerated corrosion;
Structural steel;
Mechanical properties;
Corrosion morphology;
Simulation method

1. Introduction

Steel structures, which are designed to be permanently exposed to corrosive environments such as industry and the marine atmosphere, always have difficulties avoiding corrosion. Corrosion changes the surface appearance of the steel and deteriorates its mechanical properties, which affects the safety and durability of the steel structure. The mechanical behaviour of corroded structural steel has been studied by many scholars through different accelerated corrosion methods such as salt spray tests, cyclic immersion corrosion, and electrolytic corrosion [1-6]. Xu [7] investigated the mechanical behaviour of rusted steel plates using the neutral salt spray method, as shown in Fig. 1(a). Chen [8] studied the degradation of the mechanical properties of corroded cables by a copper accelerated acetic acid salt spray test (Fig. 1(b)). Ma [9] investigated the effect of pitting corrosion by using galvanic accelerated corrosion on the seismic performance of NV-D36 steel, as shown in Fig. 1(c).

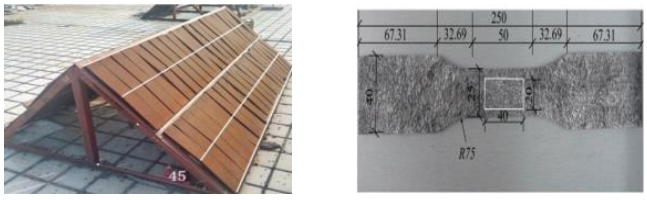

(a) Neutral salt spray corrosion

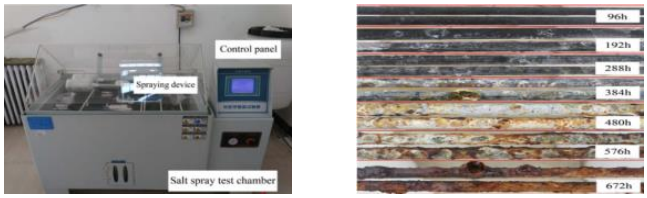

(b) Acid salt spray test

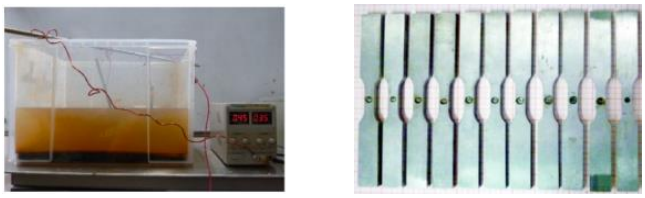

(c) Electrolytic corrosion

Fig. 1 Experimental Research on Corroded Steel

In addition to electrolytic accelerated corrosion, it may take 60-120 days to achieve a 10% mass loss of steel using other accelerated corrosion methods. A long time is required to obtain corroded steel specimens, which is not conducive to the study of corroded steel. Existing studies have shown that the stress concentration due to the uneven corrosion morphology of corroded steel surfaces is a major factor in the degradation of the mechanical properties of steel materials [10]. Compared with salt spray corrosion and cyclic immersion corrosion, the electrolytic accelerated corrosion method can greatly reduce the corrosion time, but the corroded surface of the specimen is relatively uniform, which cannot reflect the true corrosion morphology [11] and limits the application of electrolytic accelerated corrosion methods.

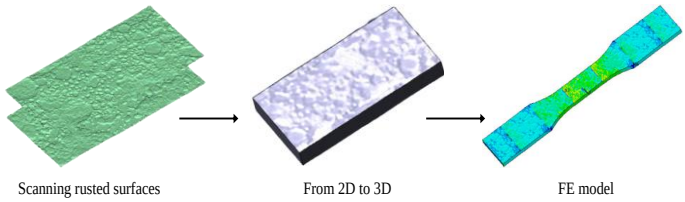

(a) Reverse modelling method

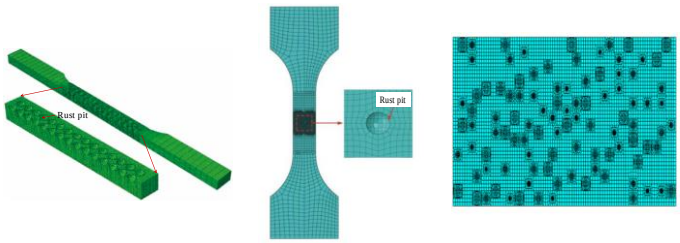

(b) Regular pits (c) Single pit (d) Random pits

Fig. 2 FE model of corroded steel

Concerning the numerical modelling of corroded steel, the existing simulation methods can be divided into two main categories [12-14]: the reverse modelling method based on the actual measurement and the method of simplifying the three-dimensional shape of pits into regular shapes. Xu [16] obtained corroded surface data by scanning a corroded steel surface with a 3D noncontact topographic scanner, importing the data into Goemagic Studio software to generate the corroded surface, building a model corresponding to the scanned area, and utilizing the finite element software ANSYS for calculation and analysis, as shown in Fig. 2(a). Xiao [17] studied the mechanical properties of corroded Q460D steel specimens based on 3D

scanning. Wang [18] simulated and analysed the ductile degradation of steel plates after corrosion damage, assuming a uniform distribution of pits, as shown in Fig. 2(b). Song [19] studied the effect of corrosion on the low-cycle fatigue performance of steel by simulating specimens with a single pit in the finite element software (Fig. 2(c)). Wang [20] performed a nonlinear analysis of 200 models by constructing a numerical model of a steel plate with random pitting damage to investigate the degradation pattern of the ultimate strength of the steel plate under random pitting damage, as shown in Fig. 2(d). Sharifi [21] studied the ultimate capacity of steel beams with pitting corrosion by artificial neural networks and analysed the safety of corroded steel box girder bridges [22]. The reverse modelling method can reflect the actual morphology of the corroded steel surface, but it heavily depends on the data obtained through scanning and is only suitable for simulating the object or area being scanned. The method of simplifying the three-dimensional shape of pits often simplifies a single pit into a regular circular or elliptical shape, and the FE model established by this method has difficulty considering the overall corrosion morphology of the corroded structure.

In this paper, an electrolytic accelerated corrosion test of steel using a suitable solution that can reflect real atmospheric corrosion was performed to obtain specimens with different corrosion degrees. Then, a 3D noncontact scanner was used to scan the surface morphology of corroded specimens to obtain the relationship between the corrosion morphology and the mass loss. A deterioration model of the mechanical properties of corroded steel was established by monotonic tensile tests. Finally, a new simulation method for corroded steel based on random rough surfaces was proposed, which was verified by comparing it with the test results.

2. Accelerated corrosion test

2.1. Test Details

Q355B is the most common and widely used steel material in steel construction in China. In this paper, Q355B structural steel was selected as the specimen material. The chemical composition of the Q355B structural steel is shown in Table 1. Tensile specimens were designed according to GB/T 228.1-2010 [23], and the geometric profile of the coupons is shown in Fig. 3.

Table 1
Q355B steel chemical composition (*wt.*%)

Material	C	Si	Mn	P	S	Alt	Fe
Q355B	0.19	0.107	0.42	0.009	0.002	0.023	Balance

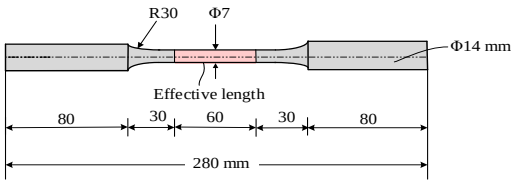

Fig. 3 Dimensional diagram of the specimen

Before the accelerated corrosion test, the specimens should be well prepared. The surface of the specimens was polished by 800#-1200# water-resistant sandpaper and subsequently cleaned with acetone. Electric wires were connected at the clamping end of the specimen and sealed with waterproof tape. In the electrolytic accelerated corrosion test, the negative electrode was made of graphite material. The two electrodes were placed 50 mm apart and symmetrically in the test container. The test container was made of acrylic, and the direct current (DC) was delivered by the SS-3010 DC power supply, as shown in Fig. 4(a). During the test, the room was kept well ventilated, and the average temperature was approximately 28 °C. The specimens and graphite were placed in the test container, as shown in Fig. 4(b).

Four groups of specimens, labelled A-D, were designed for electrolytic accelerated corrosion testing, and the durations of electrolytic accelerated corrosion were 2.5, 5.0, 7.5, and 10.0 hours, respectively. The electrolytic corrosion solution was a mixture of 0.2% NaCl and 5% CH_3COONa, which could make the steel after electrolytic accelerated corrosion form a corrosion morphology corresponding to actual atmospheric corrosion [24]. The current density of the accelerated corrosion was controlled at 400 A/m^2.

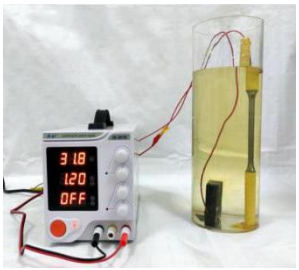

(a) Power supply and container (b) Schematic diagram of the current

Fig. 4 Electrolytic accelerated corrosion test

2.2. Results of accelerated corrosion

After electrolytic accelerated corrosion, the mass loss was used to express the degree of corrosion of the specimens. The mass loss of the specimens was recorded as w and calculated with Eq. (1). For all corroded specimens, the derusting process was performed before the loading test with 500 ml HCl (ρ=1.19 g/ml), 3.5 g $C_6H_{12}N_4$, and 500 ml distilled water following GB/T 16545-2015 [25]. A precise electronic balance with an accuracy of 0.001 g was employed to measure and record the initial weight of the specimens and the weight of the specimens after the electrolytic accelerated corrosion test.

$$w = \frac{\Delta m}{m_1} \times 100\% \tag{1}$$

where m_1 is the initial mass, m_2 is the mass of the specimen after rust removal, and Δm is the changing mass of the specimen, $\Delta m = m_1 - m_2$.

The mass loss of the four specimen groups is listed in Table 2. The results show that the corrosion degree (w) of electrolytic corrosion is linearly related to the duration of the test. The uncorroded specimen is recorded as N, and the macroscopic corrosion morphologies of specimens A1, B1, C1, and D1 are shown in Fig. 5. When the mass loss reaches 6.88%, small corrosion pits appear on the surface of the specimen, and there is no obvious change in geometric size of the specimen. When the mass loss increases, the range of corrosion gradually expands, and circular pits begin to combine to form long strips and large round pits. When the mass loss reaches 23.97%, corrosion pits continue to develop and expand, and the entire corrosion state is developed.

Fig. 5 Macro corrosion morphology of the specimens

Table 2
Mass loss of electrolytic accelerated corrosion

Duration (h)	Groups	Specimen	Δm (g)	w (%)	Average Δm (g)	Average w (%)
2.5	A	A1	3.065	6.87	3.068	6.88
		A2	3.072	6.89		
		A3	3.067	6.88		
5.0	B	B1	6.235	13.98	6.168	13.83
		B2	6.158	13.81		
		B3	6.11	13.70		
7.5	C	C1	9.168	20.56	9.177	20.58
		C2	9.193	20.62		
		C3	9.17	20.56		
10.0	D	D1	10.802	24.22	10.687	23.97
		D2	10.65	23.88		
		D3	10.608	23.79		

3. Corrosion morphology

3.1. Corrosion morphology scanning

A three-dimensional noncontact surface profiler ST-400 was adopted to scan the surface morphology of each specimen after removing the rust, as shown in Fig. 6(a). Round specimens were adopted, and any position in the gauge length had equal probability of being affected by corrosion, so each test piece was scanned twice along the axis of the specimen to characterize the roughness of the corroded specimen. The scanning lines are shown in Fig. 6(b). For simplicity, only the scanning results of specimens A1, B1, C1, and D1 are shown in Fig. 7.

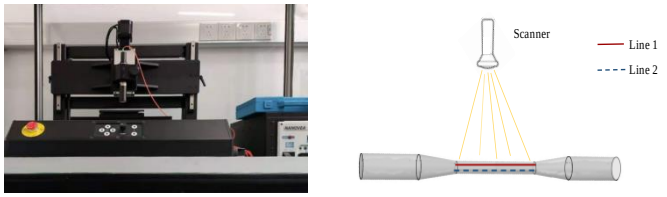

(a) 3D scanner (b) Scanned area

Fig. 6 Morphological scanning of specimens

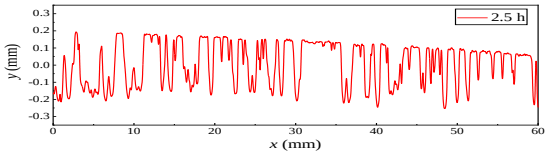

(a) A1

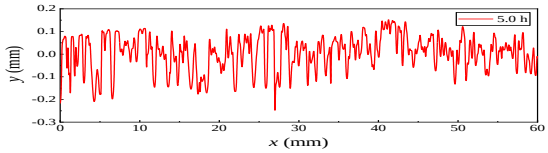

(b) B1

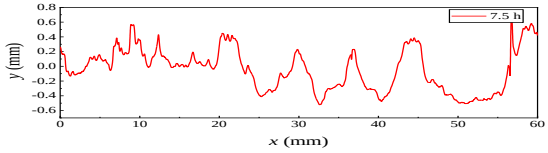

(c) C1

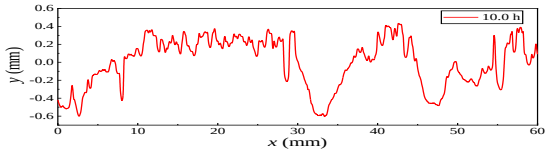

(d) D1

Fig. 7 Scanning results of some specimens

3.2. Roughness variation patterns

The surface of the corroded steel was characterized by the arithmetic average height (R_a), root mean square height (R_q), and maximum height (R_z) in the roughness theory [26]. The specific calculation formulas for each parameter are shown in Eqs. (2)-(4).

$$R_a = \frac{1}{l}\int_0^l |Z(x)|\,dx \tag{2}$$

$$R_q = \sqrt{\frac{1}{l}\int_0^l Z^2(x)dx} \tag{3}$$

$$R_z = R_p + R_v \tag{4}$$

where $Z(x)$ is the scanning surface of the specimen; R_p is the maximum peak height; R_v is the maximum valley depth; l is the side length of the sampling area. Based on the scanning results, R_a, R_q, and R_z were calculated and recorded in Table 3.

Table 3
Values of R_a, R_q, and R_z of the specimens

Specimens	R_a (mm)	R_q (mm)	R_z (mm)
A1	0.075	0.09	0.371
	0.060	0.074	0.399
A2	0.078	0.09	0.447
	0.075	0.085	0.371
A3	0.074	0.089	0.421
	0.071	0.081	0.385
B1	0.105	0.122	0.49
	0.084	0.106	0.606
B2	0.097	0.117	0.582
	0.085	0.098	0.631
B3	0.098	0.119	0.553
	0.083	0.103	0.622
C1	0.145	0.193	1.173
	0.144	0.186	0.965
C2	0.154	0.187	0.859
	0.161	0.208	1.232
C3	0.157	0.191	0.925
	0.163	0.211	1.383
D1	0.229	0.269	1.04
	0.187	0.249	1.859
D2	0.192	0.253	1.706
	0.174	0.201	1.245
D3	0.181	0.225	1.556
	0.232	0.27	1.704

The average mass loss and surface parameters of each group are shown in Table 4. The results of the average mass loss and surface parameters were fitted, as shown in Fig. 8.

Table 4
Average mass loss and average surface parameters

Groups	w (%)	R_a (mm)	R_q (mm)	R_z (mm)
A	6.88	0.072	0.085	0.399
B	13.83	0.092	0.111	0.581
C	20.58	0.154	0.196	1.090
D	23.97	0.199	0.245	1.518

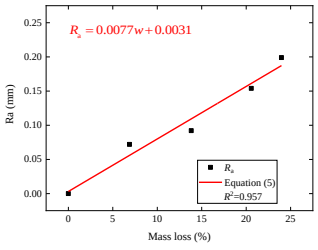

(a) R_a

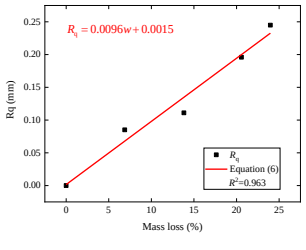

(b) R_q

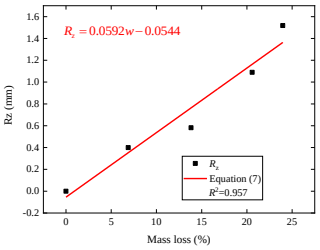

(c) R_z

Fig. 8 Relationship between surface parameters and mass loss

Fig. 8 shows that the arithmetic average height (R_a), root mean square height (R_q), and maximum height (R_z) of the one-dimensional roughness parameters of the corroded steel surface are linearly related to the mass loss and satisfied in Eqs. (5)-(7).

$$R_a = 0.0077w + 0.0031 \quad (5)$$

$$R_q = 0.0096w + 0.0015 \quad (6)$$

$$R_z = 0.0592w - 0.0544 \quad (7)$$

4. Mechanical behaviour tests under monotonic tensile loading

4.1. Mechanical behaviour tests

A monotonic tensile loading test was performed on all corroded steel specimens, as shown in Fig. 9. The tensile test was controlled by the strain. The strain loading rate was 0.00025/s according to GB/T228.1-2010, which was 0.75 mm/min.

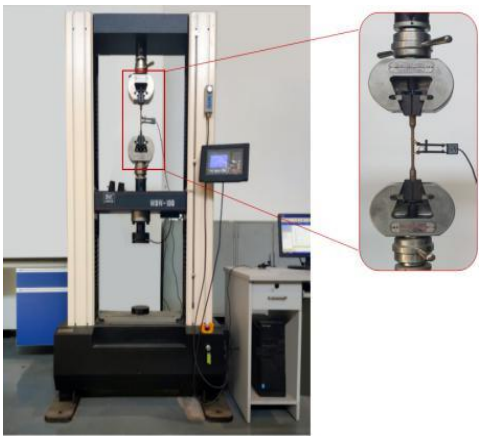

Fig. 9 Tensile test

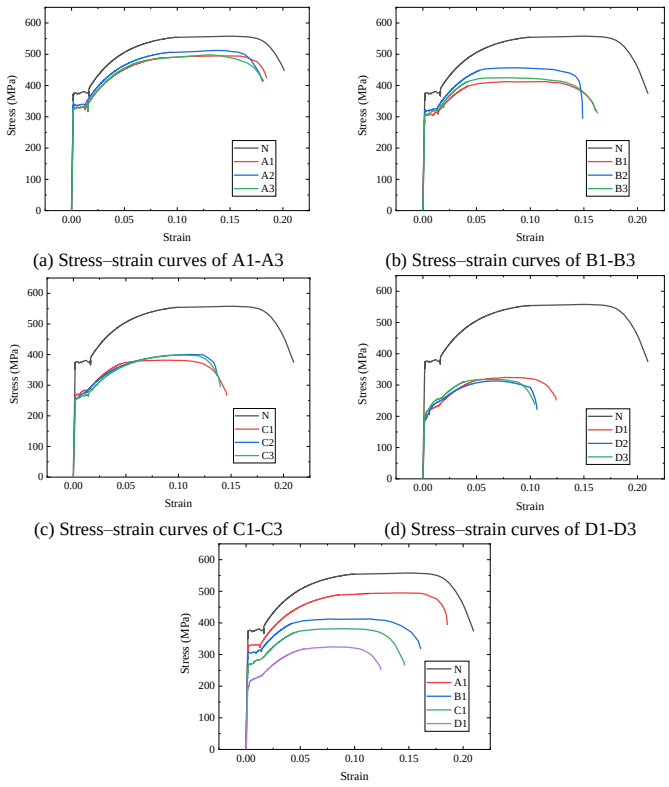

(a) Stress–strain curves of A1-A3

(b) Stress–strain curves of B1-B3

(c) Stress–strain curves of C1-C3

(d) Stress–strain curves of D1-D3

(e) Stress–strain curves of A1-D1

Fig. 10 Stress–strain curves of corroded steel

In this study, nominal stresses were adopted, and the ratio of the magnitude of the actual load to the initial cross-sectional area of the specimen was adopted to obtain the stress value. The stress–strain curves of specimens with different corrosion degrees were obtained by tensile tests, as shown in Fig. 10. The mechanical behaviour parameters of the individual specimens obtained from the tests were sorted out, and the results are shown in Table 5, where F_y is the yield capacity of the specimen, F_u is the ultimate capacity, f_y is the yield stress, f_u is the tensile stress, ε_u is the fracture strain, and E is the elastic modulus.

The influence of different corrosion degrees on the mechanical properties of Q355B steel was compared and analysed. From Table. 5, the mechanical properties of corroded specimens declined to varying degrees compared to those of uncorroded specimens, with a maximum reduction of 38.6% in yield strength, 44.0% in ultimate strength, and 52.4% in fracture strain when the degree of corrosion reaches 23.97%, which indicates that corrosion significantly affects the mechanical properties of Q355B structural steel. Interestingly, the nominal stress–strain curves of Groups A and B presented a similar behaviour to the uncorroded specimens, which contained an evident yield plateau. However, with the increase in corrosion damage, the yield plateau continued fading away, and no yield plateau was found in the stress–strain curves of the specimens in Groups C and D.

Table 5
Mechanical properties of corroded steel

Specimens	F_y (*kN*)	F_u (*kN*)	f_y (MPa)	f_u (MPa)	ε_u	E (10^5MPa)
N	14.67	21.46	381.2	557.7	0.21	2.12
A1	12.79	19.04	332.3	494.7	0.19	1.94
A2	13.10	19.71	340.3	512.2	0.18	2.03
A3	12.94	19.17	336.2	498.1	0.19	1.97
B1	12.07	15.87	313.6	412.3	0.16	2.00
B2	12.51	17.43	325.0	452.8	0.15	1.85
B3	12.37	16.33	321.3	424.2	0.16	1.88
C1	10.92	14.64	283.8	380.5	0.15	1.76
C2	10.82	15.38	281.2	399.7	0.14	1.75
C3	11.07	15.26	287.6	396.4	0.14	1.77
D1	9.00	12.47	233.9	323.9	0.13	1.44
D2	9.29	12.03	241.5	312.5	0.11	1.49
D3	9.92	12.08	257.8	313.8	0.10	1.50

4.2. Fracture analysis

The strain at break of the uncorroded specimens is nearly 20%, the section shrinkage is high, and the ductility is good. The tensile process of the corroded steel specimen is approximately identical to that of the uncorroded specimen, which follows a tensile-necking-fracture process. Due to the reduced cross-sectional area of the corroded specimen, necking and fracture occur at the pitting, and the fracture shows a fibrous shape. The specimen has no obvious sound at fracture, and the strain is large, so the corroded specimen was still determined to be a ductile fracture.

According to the metal inspection method of microstructure, metallographic specimens were cut out of the fractured specimens with a line cutting machine and polished. The specimens were subjected to microscopic observation of the metallographic organization using a Leica metallographic microscope, which magnified the specimens 1000 times, and the metallographic organization of the fractured specimens is shown in Fig. 11.

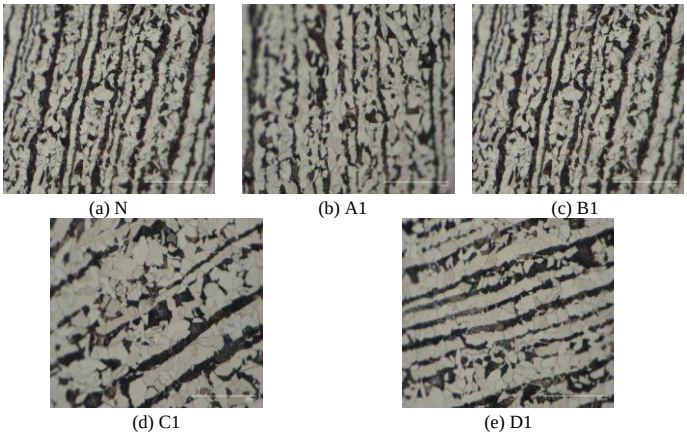

(a) N (b) A1 (c) B1

(d) C1 (e) D1

Fig. 11 Metallographic organization diagram

From Fig. 11, both uncorroded and corroded specimens are composed of white pre-eutectic ferrite and grey–black pearlite. The tissue distribution of uncorroded and corroded specimens reflects that ferrite and pearlite have identical distribution characteristics: ferrite and pearlite are distributed in strips, and the interface between pearlite and ferrite is obvious, which indicates that corrosion does not affect the tissue structure of steel, and the decrease in mechanical properties of corroded steel is mainly due to the stress concentration caused by the uneven corrosion. The existence of corrosion pits makes the specimens discontinuous. Under the action of axial tensile force, the stress concentrations occurred near corrosion pits, which caused unequal tensile stresses and increased the local strain rate in the corrosion pits. The presence of corrosion pits can easily cause the steel to be in a more brittle state, which causes the formation and progressive development of microcracks around the pits and ultimately deteriorates the mechanical properties of the steel.

4.3. Degradation law of mechanical properties

The mechanical behaviour of the corroded Q355B structural steel was analysed. The average values for each group of specimens are shown in Table 6.

Table 6
Average mechanical properties of corroded steel

Groups	f_y (MPa)	f_u (MPa)	ε_u	E (10^5MPa)
N	381.2	557.7	0.21	2.12
A	336.3	501.7	0.19	1.98
B	320.0	429.8	0.16	1.91
C	284.2	392.2	0.14	1.76
D	244.4	316.7	0.11	1.48

The yield strength of corroded steel is recorded as f_y', the ultimate strength is f_u', the strain at fracture is ε_u', and the modulus of elasticity is E'. The ratio of the mechanical properties of corroded Q355B structural steel to the initial uncorroded state is shown in Table 7 and Fig. 12.

Table 7
Ratio of the mechanical properties of corroded steel to its initial state

Groups	f_y'/f_y	f_u'/f_u	$\varepsilon_u'/\varepsilon_u$	E'/E
A	0.88	0.90	0.89	0.93
B	0.84	0.77	0.75	0.90
C	0.75	0.70	0.68	0.83
D	0.64	0.57	0.54	0.70

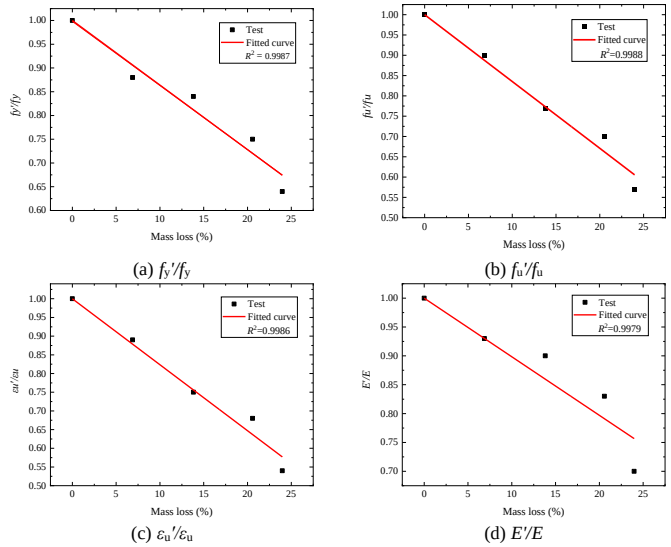

Fig. 12 Changes in the mechanical properties of corroded steel

Fig. 12 shows that the yield strength, ultimate strength, fracture strain, and elastic modulus of the steel decrease when the mass loss increases, and the following equations are fulfilled:

$$f_y'/f_y = 1 - 0.01359w \tag{8}$$

$$f_u'/f_u = 1 - 0.01646w \tag{9}$$

$$\varepsilon_u'/\varepsilon_u = 1 - 0.01765w \tag{10}$$

$$E'/E = 1 - 0.01015w \tag{11}$$

5. Modelling methods based on surface morphology

5.1. Modelling process based on surface morphology

The existing numerical modelling methods for corroded steel have two problems: it is completely based on measured data, and the corrosion pit is simplified to a circular or oval shape, which ignores the overall morphology of the corroded surface.

In this study, the surface of corroded steel is considered a two-dimensional random rough surface, as shown in Fig. 13, where the shaded areas represent the corrosion part, and the blue region is the steel matrix. The area between the highest and lowest points on the corroded surface is recorded as S_1, the distance from the lowest point on the corroded surface to the centerline is recorded as b, and the area covered is recorded as S_2. The radius of the specimen in its uncorroded state is recorded as r, and the diameter is recorded as d.

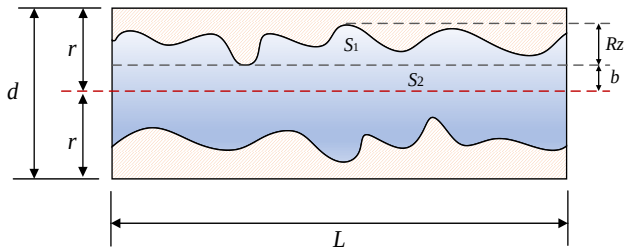

Fig. 13 Two-dimensional model of corroded steel

The Monte Carlo method was used to generate a one-dimensional randomly rough surface corresponding to the mass loss. In this paper, the length (L) of the generated one-dimensional curve is equal to the effective length in Fig. 1, which is 60 mm. The interval of adjacent data points is 0.01 mm, i.e., each model contains 6000 data points. Next, the distance from the lowest point of the corroded surface to the centreline was calculated. Finally, the obtained one-dimensional rough surface was combined with other surfaces to produce a corroded steel model, as shown in Fig. 14.

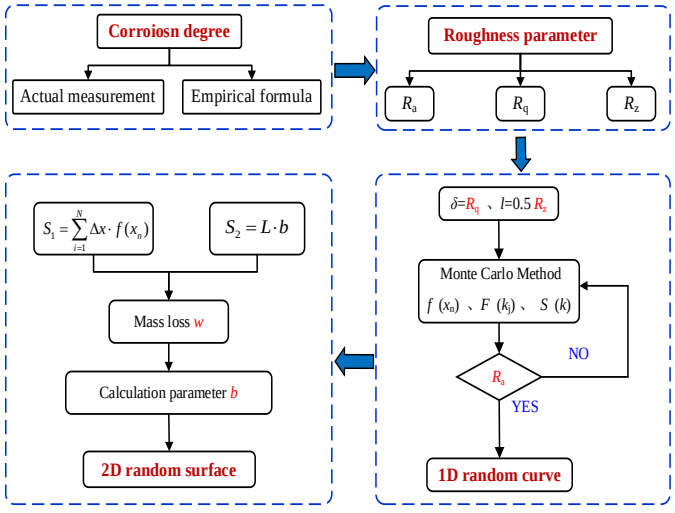

Fig. 14 Flowcharts of modelling methods

For a one-dimensional randomly rough surface, a one-dimensional rough surface sample [27] with length L and data point N is generated by Eq. (12).

$$f(x_n)=\frac{1}{L}\sum_{j=-N/2+1}^{N/2}F(k_j)e^{ik_jx_n} \tag{12}$$

where $x_n=n$. Δx is the nth sample point on the rough surface, and $F(k_j)$ and $f(x_n)$ are called Fourier transform pairs and defined as:

$$F(k_j)=\left[2\pi LS(k_j)\right]^{1/2}\cdot\begin{cases}[N(0,1)+iN(0,1)]/\sqrt{2} & j\neq 0,N/2\\ N(0,1) & j=0,N/2\end{cases} \tag{13}$$

$S(k_j)$ is the power spectral density of the rough surface; $N(0,1)$ is the random number of a normal distribution with mean 0 and variance 1; δ is the height of the root mean square; l is the correlation length.

The power spectrum [28] corresponding to the one-dimensional Gaussian rough surface is:

$$S(k)=\frac{\delta^2 l}{2\sqrt{\pi}}\exp\left(\frac{-k^2l^2}{4}\right) \tag{14}$$

When generating a one-dimensional randomly rough surface with the Monte Carlo method, the root mean square height (δ) and associated length (l) were involved, R_q was calculated using Eq. (6), and R_z was calculated using Eq. (7) with $\delta=R_q$ and $l=0.5R_z$.

According to Fig. 13, in the simplified model of steel after corrosion, S_1 and S_2 are calculated as follows:

$$S_1=\sum_{i=1}^{N}\Delta x\cdot f(x_n) \tag{15}$$

$$S_2=L\cdot b \tag{16}$$

Based on Eq. (15) and Eq. (16), the mass loss (w) can be expressed as:

$$w=1-\frac{S_1+S_2}{r\cdot L}\times 100\% \tag{17}$$

The formula of b is:

$$b=\frac{r\cdot L\cdot(1-w)-\sum_{i=1}^{N}\Delta x\cdot f(x_n)}{L} \tag{18}$$

The calculation was performed in MATLAB software using the loop command to generate the one-dimensional random curve, and the value of R_a calculated by Eq. (5) was used as a criterion for determination. When the mean square height of the generated curve satisfies the condition, the generated curve was output, and the loop stopped. The one-dimensional roughness curve corresponding to the specimens in the accelerated corrosion test obtained by the above method is shown in Fig. 15.

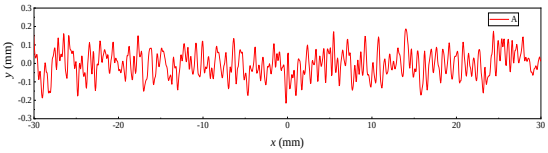

(a) Curves corresponding to group A

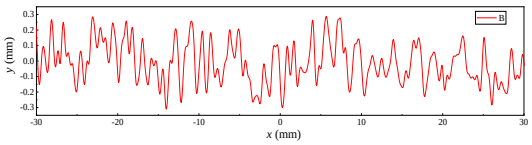

(b) Curves corresponding to group B

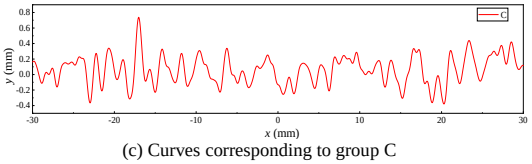

(c) Curves corresponding to group C

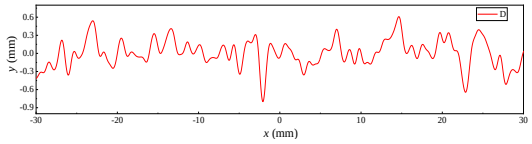

(d) Curves corresponding to group D

Fig. 15 One-dimensional random rough curves

5.2. Calculation and analysis of the FE model

After obtaining the random curve of the corroded surface corresponding to the mass loss, distance b from the lowest point in the corroded surface to the centerline was calculated using the above algorithm. The FE model corresponding to the specimen obtained from the accelerated corrosion test is shown in Fig. 16. The FE models corresponding to the electrolytic corrosion tests were denoted as FE-A, FE-B, FE-C, and FE-D. The model corresponding to the uncorroded specimen was recorded as FE-N.

In the FE model, the boundary conditions were fixed on the left side, and a reference point was established on the right side. This point was coupled with the right side surface, and displacement was loaded at this point. Taking the FE-A model as an example, its specific boundary conditions are shown in Fig. 17.

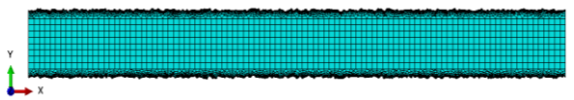

(a) FE-A

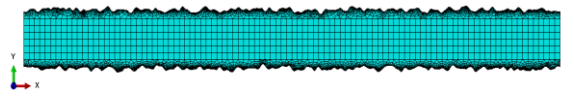

(b) FE-B

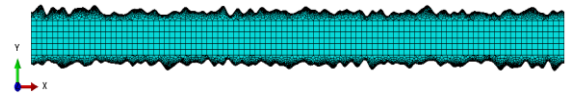

(c) FE-C

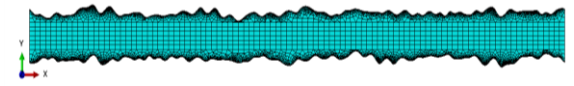

(d) FE-D

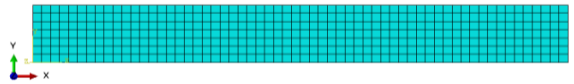

(e) FE-N

Fig. 16 Two-dimensional FE model of corroded steel

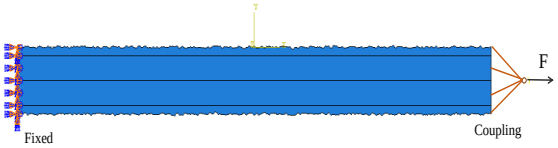

Fig. 17 Schematic boundary conditions

The material constitutive adopted in each FE model was the stress – strain relationship of steel without corrosion, and the static general analysis step was used to solve the model. The strain corresponding to the stress was reduced to 85% of the ultimate stress as the fracture strain. The stress – strain curve of each model is shown in Fig. 18.

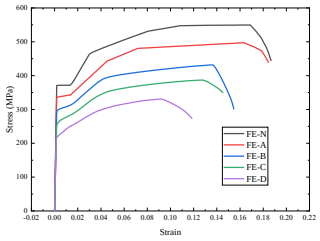

Fig. 18 Stress–Strain Curve of FE Models

5.3. Comparison and validation of results

The stress–strain curves obtained by the finite element models were compared with the tensile test, as shown in Fig. 19. Fig. 20 shows the comparison of various mechanical parameters calculated by finite element with Eqs. (8)-(11).

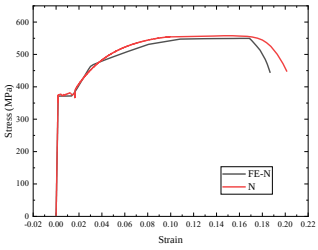

(a) Stress–strain curves of group N

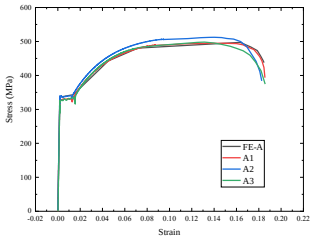

(b) Stress–strain curves of A1-A3

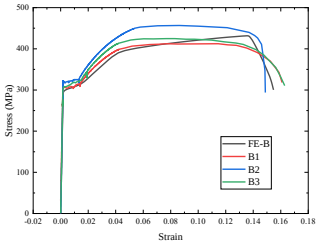

(c) Stress–strain curves of B1-B3

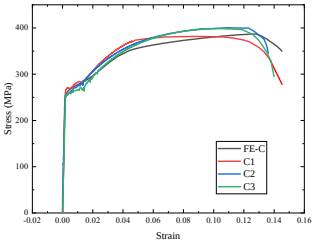

(d) Stress–strain curves of C1-C3

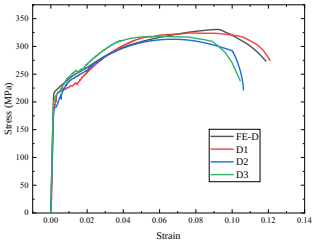

(e) Stress–strain curves of D1-D3

Fig. 19 Comparison diagram of the stress–strain curve

The comparative diagram shows that the FE model has consistent results with the experimental test, which indicates that the mechanical behaviour of the steel calculated by the FE model is consistent with the tensile test and confirms the feasibility and accuracy of the proposed method based on surface morphology.

References

[1] Xiao L, Peng J, Zhang J, et al. Comparative assessment of mechanical properties of HPS between electrochemical corrosion and spray corrosion[J]. Construction and Building Materials. 2020, 237: 117735.
[2] Wu H, Lei H, Chen Y F, et al. Comparison on corrosion behaviour and mechanical properties of structural steel exposed between urban industrial atmosphere and laboratory simulated environment[J]. Construction and Building Materials. 2019, 211: 228-243.
[3] Xu S, Zhang Z, Li R, et al. Effect of cleaned corrosion surface topography on mechanical properties of cold-formed thin-walled steel[J]. Construction and Building Materials. 2019, 222: 1-14.
[4] Zhang C, Zhu H, Zhu L. Effect of interaction between corrosion and high temperature on mechanical properties of Q355 structural steel[J]. Construction and Building Materials. 2020: 121605.
[5] Rajput A, Paik J K. Effects of naturally-progressed corrosion on the chemical and mechanical properties of structural steels[J]. Structures. 2020.
[6] Jia C, Shao Y, Guo L, et al. Incipient corrosion behavior and mechanical properties of low-alloy steel in simulated industrial atmosphere[J]. Construction and Building Materials. 2018, 187: 1242-1252.
[7] Xu S, Wang H, Li A, et al. Effects of corrosion on surface characterization and mechanical properties of butt-welded joints[J]. Journal of Constructional Steel Research. 2016, 126: 50-62.

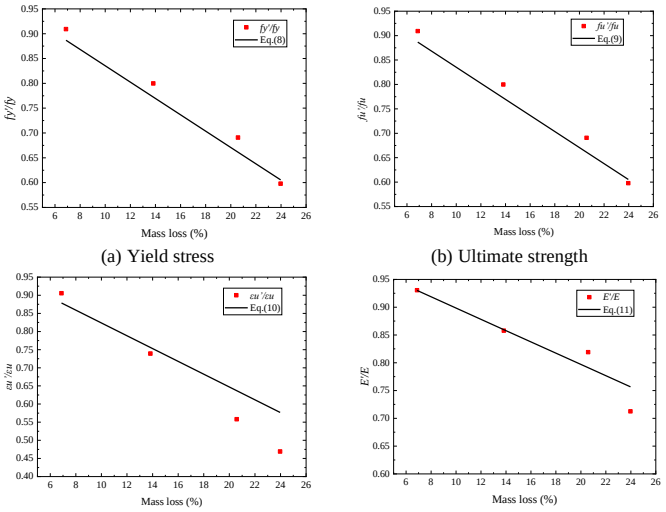

(a) Yield stress (b) Ultimate strength

(c) Fracture strain (d) Elastic modulus

Fig. 20 Comparison diagram of the FE model and tests

6. Conclusion

Based on structural steel Q355B, the surface morphology, mechanical behaviour, and simulation method of corroded structural steel were studied. A model to calculate the surface morphological parameters of steel with mass loss was developed. The degradation law of the mechanical behaviour of corroded steel was obtained. A novel simulation method of corroded steel based on random rough surface theory was proposed. The main conclusions are as follows:

(1) As corrosion develops, an uneven corrosion morphology gradually appears on the steel surface. The arithmetic average height (R_a), root mean square height (R_q), and maximum height (R_z) of the corroded steel surface are linearly related to the mass loss, which increases when the mass loss increases.

(2) The uneven corrosion morphology may cause concentrated localized stress, which results in a nonuniform distribution of stresses under axial tension. When the corrosion degree increases, the yielding platform of the steel gradually disappears, and the yield strength, ultimate strength, fracture strain, and elastic modulus of the steel decrease.

(3) By simplifying the corroded steel into a two-dimensional random rough surface and combining the surface morphology parameters of the corroded surface, the method based on the random rough surface theory can be used to establish the FE model corresponding to various corrosion degrees. The validity of the simulation method was verified by comparing the simulated results with experimental tests.

Acknowledgement

The reported research work was sponsored by the National Key Research and Development Program of China (2018YFC1504304).

[8] Chen, Z., Chen, H., Liu, H., and Yang, S. Corrosion behavior of different cables of large-span building structures in different environments. Journal of Materials in Civil Engineering. 2020, 32: 04020345.
[9] Ma H, Yang Y, He Z, et al. Experimental study on mechanical properties of steel under extreme cyclic loading considering pitting damage[J]. Ocean Engineering. 2019, 186: 106091.
[10] Xu, S., Wang, H., Li, A., Wang, Y., and Su, L. Effects of corrosion on surface characterization and mechanical properties of butt-welded joints. Journal of constructional steel research. 2016, 126: 50-62.
[11] Yuan, Y., Zhang, X., and Ji, Y. A comparative study on structural behavior of deteriorated reinforced concrete beam under two different environments. China civil engineering journal. 2006, 39: 42-46.
[12] Zheng Y, Wang Y. Damage evolution simulation and life prediction of high-strength steel wire under the coupling of corrosion and fatigue[J]. Corrosion Science. 2020, 164: 108368.
[13] Wang H, Zhang Z, Qian H, et al. Effect of local corrosion on the axial compression behavior of circular steel tubes[J]. Engineering Structures. 2020, 224: 111205.
[14] Jasra Y, Singhal S, Upman R, et al. Finite element simulation of stress corrosion cracking in austenitic stainless steel using modified Lemaitre damage model[J]. Materials Today: Proceedings. 2020, 26: 2314-2322.
[15] Zhao Z, Zhang H, Xian L, et al. Tensile strength of Q345 steel with random pitting corrosion based on numerical analysis[J]. Thin-Walled Structures. 2020, 148: 106579.
[16] Xu Shanhua, Wang Hao, Su Lei, et al. Ductility degradation of corroded steel plates with pitting damage[J]. 2016, 46(6): 1257-1263. (In Chinese)
[17] Xiao L F, Peng J X, Zhang J R, et al. Mechanical properties of corroded high performance

steel specimens based on 3d scanning[J]. Advanced Steel Construction. 2019, 15(2): 129-136.
[18] Wang Y, Shi T, Zhang H, et al. Hysteretic behavior and cyclic constitutive model of corroded structural steel under general atmospheric environment[J]. Construction and Building Materials. 2020: 121474.
[19] Song F , Xie X .Effect analysis of corrosion on low cycle fatigue behavior of structural steel. Journal of Zhejiang University (Engineering Science) . 2018, 52(12): 2285-2294. (In Chinese)
[20] Wang R, Ajit Shenoi R, Sobey A. Ultimate strength assessment of plated steel structures with random pitting corrosion damage[J]. Journal of Constructional Steel Research. 2018, 143: 331-342.
[21] Sharifi Y, Tohidi S. Ultimate capacity assessment of web plate beams with pitting corrosion subjected to patch loading by artificial neural networks[J]. Advanced Steel Construction. 2014, 10(3): 325-350.
[22] Sharifi Y, Paik J, et al. Safety analysis of steel box girder bridges with pitting corrosion[J]. Advanced Steel Construction. 2016,12(4): 359-379.
[23] GB/T 228.1, Tensile Test of Metallic Materials Part 1: Room Temperature Test Method, Standards Press of China, Beijing, 2010. (In Chinese)
[24] Si Q, Ding Y, Zong L. Electrolytic Accelerated Corrosion Morphology for Structural Steel based on an improved solution. Corrosion Reviews. 2021, 39(4):373-386.
[25] GB/T 16545, Corrosion of metals and alloys - Removal of corrosion products on corrosion specimens, Standards Press of China, Beijing, 2012. (In Chinese)
[26] ISO 25178-2: Geometrical product specifications (GPS) - Surface texture: Areal Part 2: Terms, definitions and surface texture parameters. 2012.
[27] Guo L . Basic theory and method of compound electromagnetic scattering between random rough surface and target[M]. Science Press, 2014. (In Chinese)
[28] Chen H, Hu Y, Wang H, et al. Computer Simulation of Rough Surfaces[J]. Lubrication Engineering. 2006(10): 52-55, 59. (In Chinese)